

Numerical modeling of failed rifts in the northern South China Sea margin: Implications for continental rifting and breakup



Yaqing Li^a, Aqeel Abbas^a, Chun-Feng Li^{a,b,*}, Tienan Sun^c, Sergio Zlotnik^d, Taoran Song^e, Lulu Zhang^a, Zewei Yao^a, Yongjian Yao^f

^a Department of Marine Sciences, Zhejiang University, Zhoushan 316021, China

^b Laboratory for Marine Mineral Resources, Qingdao National Laboratory for Marine Science and Technology, Qingdao 266237, China

^c Tongji University, Shanghai 200092, China

^d Universitat Politècnica de Catalunya, Barcelona 08034, Spain

^e School of Marine Science and Technology, Hainan Tropical Ocean University, Sanya 572022, China

^f Guangzhou Marine Geological Survey, Guangzhou 510075, China

ARTICLE INFO

Keywords:

Failed rifts
Continental breakup
Rift competition
Rift migration
Extension rate
Numerical modeling

ABSTRACT

Failed rifts record important information of continental extension and breakup process in the northern South China Sea (SCS) margin. The Tainan Southern Depression and the Baiyun Sag to the east are characterized with lower-crust high-velocity anomalies (LCHVA), and intracrust detachment faults, whereas the Xisha Trough to the west develops on a larger scale with crust-cutting normal faults and absence of LCHVA. These contrasts indicate different rifting processes between the northeastern and northwestern SCS. 2D numerical modeling is performed to understand the formation mechanism of these failed rifts. Two types of mechanisms are proposed: I) syn-rift competitive type and II) rift migration type with a half extension rate of 2 cm/yr and 1.5 cm/yr, respectively. In type I, two rifts develop initially on the shoulders of the weak zone, but they compete with each other during extension. One rift becomes dominant to furnish the final breakup, whereas the other one is abandoned. The crust structure of this type fits the observations in the Baiyun Sag and the Tainan Southern Depression. However, in type II, only one rift develops at the beginning. The initial rifting center will migrate and the final continental breakup will occur at a place far from the initial rifting location. In this type, normal faults cut through whole crust and wide extensional margins will form, such as observed in the Xisha Trough. Our results suggest that the depth-dependent extension of the SCS is strongly heterogeneous, resulting primarily from varying extensional rates.

1. Introduction

Failed rifts, also called aborted or abandoned rifts, are domains of hyper-extended continental lithosphere, where mantle exhumation may occur, but no oceanic crust is generated (Hauser et al., 1995; McIntosh et al., 2014; O'Reilly et al., 1996). They record abundant information on continental rifting and breakup process (Lei and Ren, 2016). Failed rifts have been detected on the North Atlantic continental margin, e.g., the Rockall Trough (Hauser et al., 1995; O'Reilly et al., 1996) and the Porcupine Basin (O'Reilly et al., 2006; Reston et al., 2004).

The SCS is one of the largest marginal basins along the West Pacific. Many failed rifts are recognized in the SCS (Fig. 1a), such as the Xisha Trough (Lei and Ren, 2016; Qiu et al., 2001; Shi et al., 2002), the Baiyun Sag (Hu et al., 2009; Nirrengarten et al., 2020; Wang et al., 2018; Zhao et al., 2018), the Tainan Southern Depression (Lester et al.,

2012; Lester et al., 2014; McIntosh et al., 2014; Yeh et al., 2012), the Phu Khanh Rift (also known as the Zhongjinnan Basin) (Cullen et al., 2010; Savva et al., 2013; Savva et al., 2014) and the East Natuna Basin (also known as the Beikang Basin) (Savva et al., 2014). In all these failed rifts, continental crust is thinned from about 35 km to ~6–8 km. In some places, like the Phu Khan Basin (Savva et al., 2014), exhumed mantle may be in direct contacts with sedimentary cover. In this study, we will focus on the failed rifts in the northern SCS margin with good seismic data coverage.

Several studies have been conducted to investigate the crustal structure, stretching factor, sediment process, subsidence history, fault activities, magnetic features and formation mechanisms of these failed rifts (Huang et al., 2005; Huang et al., 2019a; Huang et al., 2019b; Lester et al., 2014; Li et al., 2007; McIntosh et al., 2014; Nirrengarten et al., 2020; Qiu et al., 2001; Wang et al., 2018; Zhao et al., 2016; Zhao

* Corresponding author at: Department of Marine Sciences, Zhejiang University, Zhoushan 316021, China.

E-mail address: cqli@zju.edu.cn (C.-F. Li).

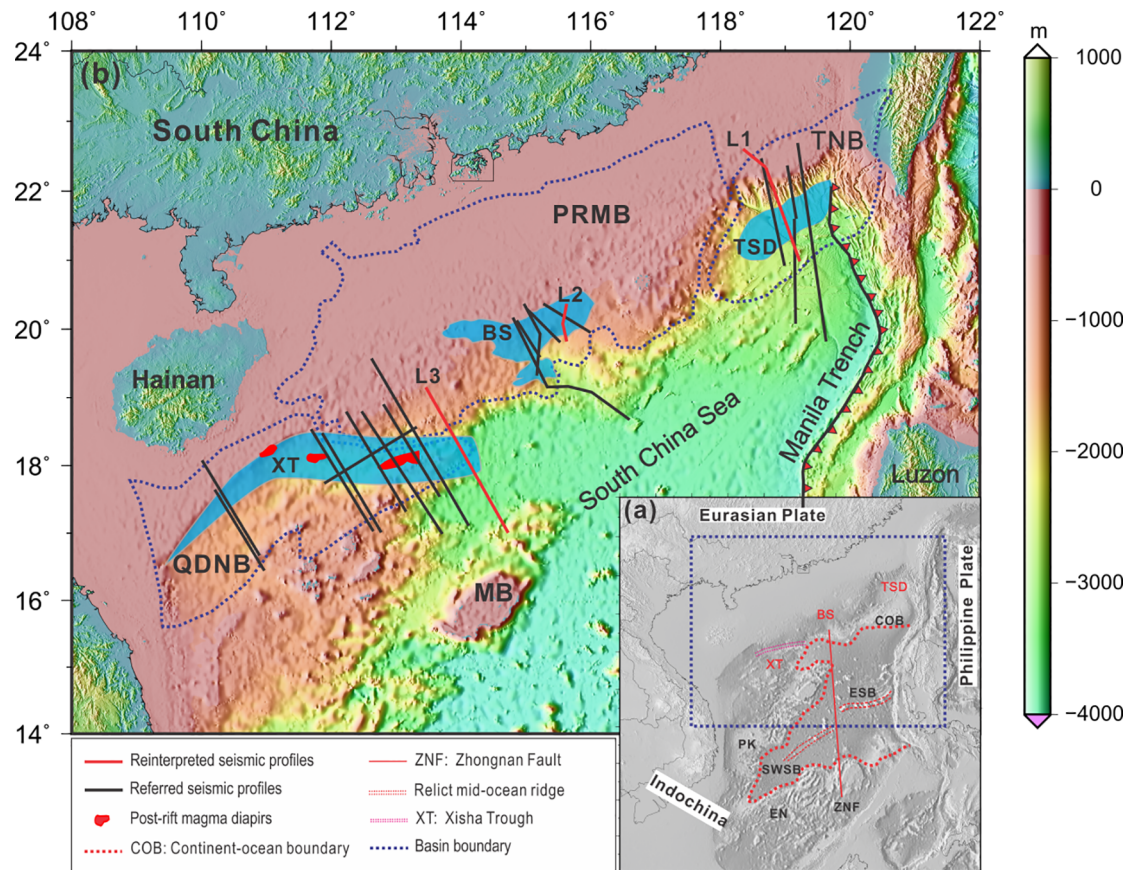


Fig. 1. (a) Map showing the location of SCS. Blue square shows the study area. (b) Map of the distribution of failed rifts along the northern SCS continental margin. From east to west are the Tainan Southern Depression (Ding et al., 2008), the Baiyun Sag (Zhao et al., 2016) and the Xisha Trough (Lei and Ren, 2016) marked by blue shaded areas. ESB: East Subbasin; SWSB: Southwest Subbasin; XT: Xisha Trough; BS: Baiyun Sag; TSD: Tainan Southern Depression; PK: Phu Khanh Rift; EN: East Natuna; MB: Macclesfield Bank; QDNB: Qiongdongnan Basin; PRMB: Pearl River Mouth Basin; TNB: Tainan Basin.

et al., 2018). Shi et al. (2002) suggested that the massive Xisha-Zhongsha Blocks hampered the Xisha Trough from breaking up. One of the key processes controlling the evolution of the Xisha Trough could be depth-dependent extension arising from regional dynamic lower crustal/mantle flow (Lei and Ren, 2016). In the hyper-extended Baiyun Sag, strong lithospheric heterogeneity and elevated temperatures probably resulted in a weak pre-rift crust with multiple decoupling and a ductile lower crust (Nirrengarten et al., 2020).

These failed rifts in the SCS are different in crustal structure. Most noticeably, the thinned northwestern continental crust where developed the Xisha Trough, is much wider than the northeastern margin, in which the Baiyun Sag and the Tainan Southern Depression are located. Differences between these failed rifts have not been well investigated, and their formation mechanisms and relationship with seafloor spreading are still unclear.

Continental extension and breakup are a long and complex process involving various thermal-mechanical dynamics, rock physical properties and rheologies. Many factors affect the rifting process, including inherited weak or strong zones, lateral variability in lithospheric structure, thermomechanical state, materials, and magmatism (Allken et al., 2011). It is difficult to understand the entire process based on field observation alone. Numerical modeling allows us to isolate different controlling parameters, and has been extensively applied to understanding the structure and magmatic evolution of rifted margins (Brune et al., 2017; Chenin and Beaumont, 2013; Huismans and Beaumont, 2003, 2011, 2014; Liao and Gerya, 2014; Pérez-Gussinyé et al., 2006; van Wijk et al., 2001).

In this study, we reviewed and compared the three failed rifts along the northern SCS margin with aspect to crustal structure, magmatism,

LCHVA and tectonic style of detachment faults. Then we investigated the major controlling factors on formation of failed rifts with 2D numerical modeling using software Gale (Moresi et al., 2003). A series of models with different extension rates, lower crust rheologies and lithospheric temperatures are performed to gain insight into continental rifting process.

2. Geology background

The SCS is surrounded by the Philippine Sea Plate, the Eurasian Plate and the Indo-Australian Plate (Fig. 1a). Before the rifting stage of the SCS, an Andean-type convergent margin had developed due to the subduction of the Paleo-Pacific Plate (Jahn et al., 1976; Li and Li, 2007). Despite its relatively small size and short evolutionary history, the SCS has undergone nearly a complete Wilson cycle from the Late Cretaceous-Paleogene continental rifting to Oligocene-middle Miocene seafloor spreading, and to eastward subduction under the Luzon arc started in the early Middle Miocene (Briais et al., 1993; Li et al., 2014; Taylor and Hayes, 1980; Taylor and Hayesb, 1983). Collision and continental underthrusting also occurred between Dangerous Grounds (Nansha Blocks) and Borneo along the Borneo Trough (Cullen, 2014; Hall, 2012).

Based on seismic and drilling data, the rifting history of the SCS can be divided into three episodes (Zhou et al., 1995). The first stage formed small basins from the Late Mesozoic to the Early Eocene. The second rifting episode took place in the middle Eocene and formed rifting basins filled with a mainly lacustrine sequence of several hundred to over 1000 m thick. Intense rifting renewed in the Late Eocene and lasted until the Late Oligocene. This episode of rifting eventually

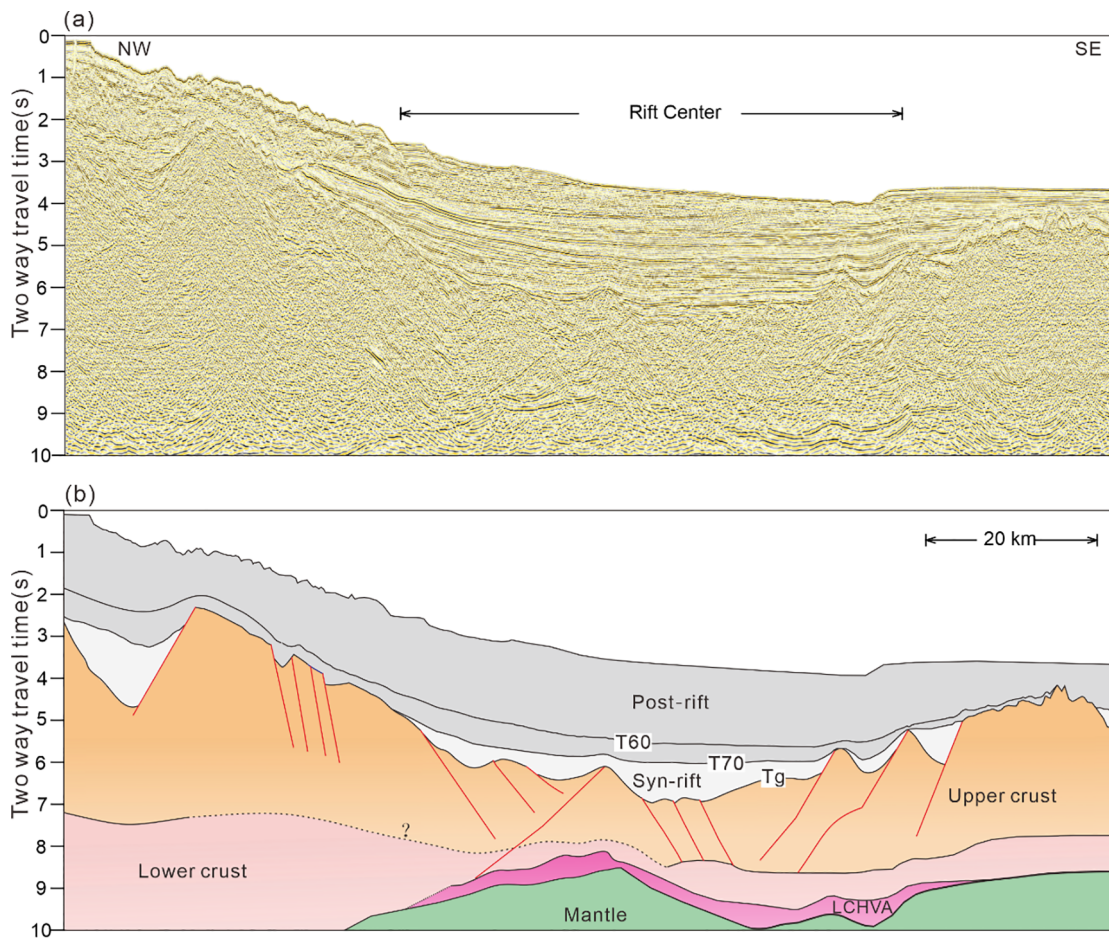


Fig. 2. (a) Seismic section L1 across the Tainan Southern Depression. (b) Geological interpretation of L1. T70: breakup unconformity in ESB (~34 Ma); T60: unconformity caused by onset of seafloor spreading in SWSB (~23.6 Ma); Tg: top basement; LCHVA: lower crust high velocity anomalies.

led to the breakup of the continental margin and the opening of the SCS (Zhou et al., 1995).

Seafloor spreading occurred between ~33 and 15 Ma (Barckhausen et al., 2014; Barckhausen and Roeser, 2004; Briais et al., 1993; Li et al., 2014; Taylor and Hayes, 1980, Taylor and Hayesb, 183)). Seafloor spreading occurred first in the East Subbasin, followed by a southward ridge jump at 23.6 Ma and opening of the Southwest Subbasin with a re-orientation of the spreading geometry (Briais et al., 1993; Li et al., 2014). Two end-member geodynamic models have been proposed, extrusion of the Indochina block bounded by the Red River-Ailaoshan Fault system (Briais et al., 1993; Tapponnier et al., 1986; Tapponnier et al., 1982) and Proto-SCS slab pull model (Clift et al., 2008; Cullen et al., 2010; Franke et al., 2008; Hall, 2002; Hinz et al., 1989; Holloway, 1982).

The hyper-extended northern SCS margin is a magma-poor margin with detachment faults but absence of seaward dipping reflectors (Gao et al., 2015; Savva et al., 2014; Yan et al., 2006; Yan et al., 2001). However, massive post-spreading volcanism and LCHVA with P-wave velocities (V_p) of 7.0–7.6 km/s have been detected (Wang et al., 2006; Yan et al., 2001). LCHVA in magma-poor margins usually come from serpentinized mantle materials (Boillot et al., 1980; Chian and Loudon, 1994; Van Avendonk et al., 2006), whereas those beneath magma-rich margins are interpreted as from magmatic underplating (Mjelde et al., 2005; Mutter et al., 1984; Voss and Jokat, 2007). LCHVA at different locations in the northern SCS margin may have multiple causes, including Cenozoic post-rifting magmatic underplating (Wang et al., 2006; Wei et al., 2011; Yan et al., 2001; Zhao et al., 2010), Mesozoic subduction-related magmatism (Wan et al., 2017), and mantle upwelling and serpentinization at the continent-ocean boundary (Hou et al.,

2019; Wan et al., 2019).

3. Characteristics of failed rifts in the northern SCS

3.1. The Tainan Southern Depression

The northeastern SCS margin consists of a wide zone of extended to hyper-extended continental crust of 300–400 km in width (Hayes and Nissen, 2005; Nissen et al., 1995a; Nissen et al., 1995b). The Tainan Southern Depression is a subunit of the Tainan Basin (Fig. 1b), which is a Late Eocene-Early Miocene extensional unit with up to 10 km of Cenozoic sedimentary fill (Ding et al., 2008).

The continental crust is thinned to ~6 km in the central valley (Lester et al., 2014). The surrounding upper crust is featured with listric and tilted fault blocks, and most of the fault planes merge into the subhorizontal upper-lower crust boundary (Fig. 2), except for a major landward-dipping boundary fault cutting through the entire crust (Li et al., 2007). Wide angle seismic profiling across the Tainan Southern Depression shows an absence of the 4.0–6.0 km/s velocity layer in the rift center (Lester et al., 2014), indicating that the upper crust may have been torn apart during the extension. A layer of relatively continuous reflection of 2–5 km thick with a velocity range of 7.0–7.5 km/s above the Moho is identified as LCHVA (Lester et al., 2014; McIntosh et al., 2014; Wang et al., 2006; Yeh et al., 2012). Syn-rift magmatic activity was weak (McIntosh et al., 2014; Yan et al., 2006), no large-scale magmatic intrusions or volcanic flows are detected in the failed rift center, but the crust further south in the distal domain is intruded by post-rift volcanoes (Lester et al., 2014; McIntosh et al., 2014).

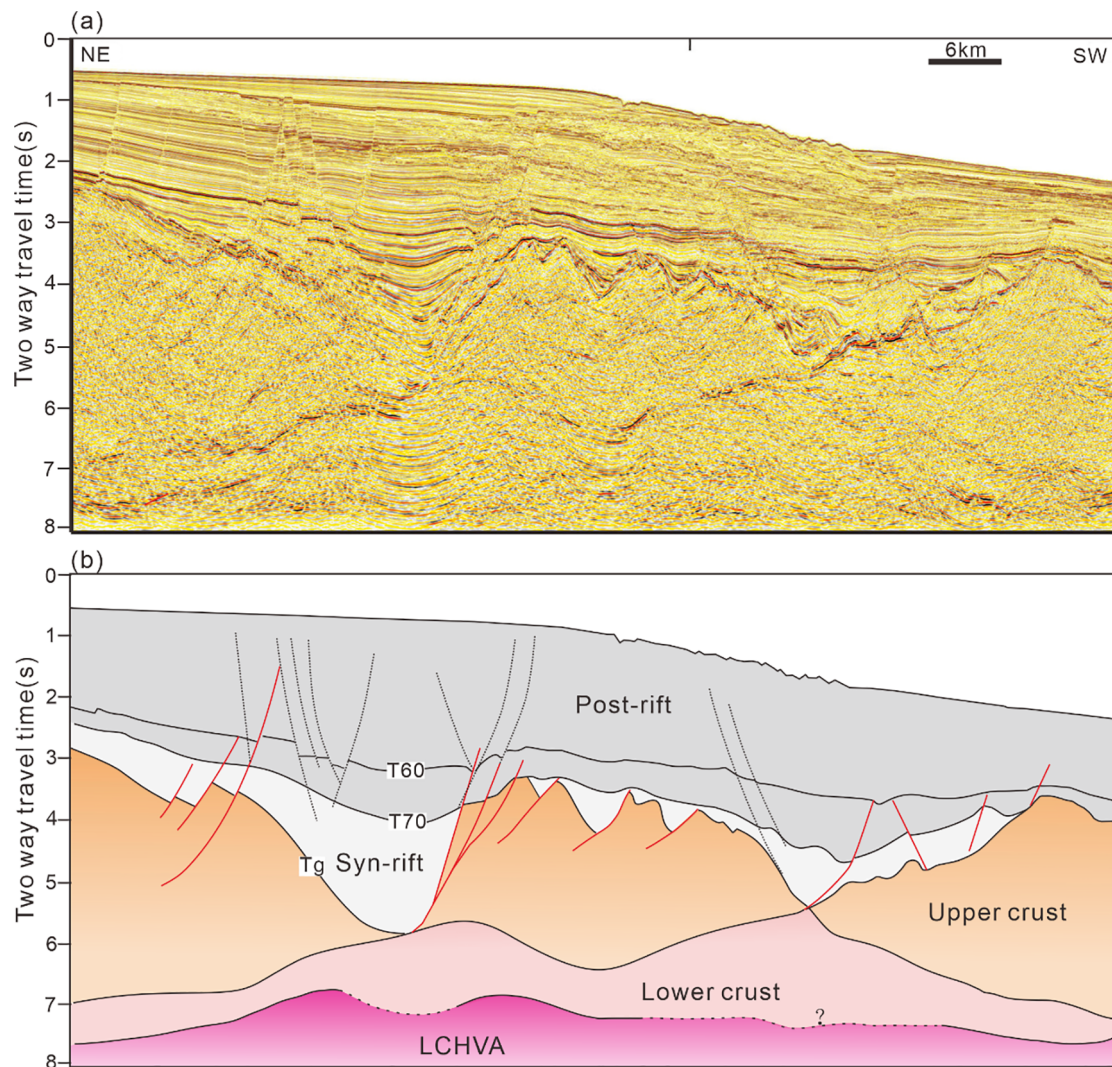


Fig. 3. (a) Seismic profile L2 across the Baiyun Sag (modified from Zhao et al., 2018). (b) Geological interpretation of L2. T70: breakup unconformity in ESB (~34 Ma); T60: unconformity caused by onset of seafloor spreading in SWSB (~23.6 Ma); Tg: top basement; LCHVA: lower crust high velocity anomalies. Black dash lines indicate post-rift faults.

3.2. The Baiyun Sag

Cenozoic sediments in the Baiyun Sag (Fig. 1b) have a maximum thickness of over 14 km (Clift et al., 2002; Huang et al., 2005). It is difficult to date the initial rifting age due to the lack of well penetration into the deep buried syn-rifting sequence (Morley, 2016). Zhou et al. (1995) argued that the initial rifting must be later than 50 Ma due to the absence of the Paleocene sequence. Shi et al. (2011) suggested that the rifting initiated in the Late Paleocene at around 59 Ma and reached a peak during the Late Eocene.

Seismic profiles across the Baiyun Sag show that the crystalline basement is at ~7.5 s in two-way travel time (TWTT) (Huang et al., 2005) and the Moho reflection is at about 9–10 s TWTT. The crustal thickness of the Baiyun Sag is estimated at about 7 km assuming a crustal velocity of 6.5 km/s. Seismic profile L2 shows that the upper crust has been intensely cut by normal faults. These faults extended downward to merge into a set of continuous reflectors at about 7.0 s (TWTT), which could be from the detachment fault along the upper-lower crust boundary (Fig. 3). Nirrengarten et al. (2020) suggested that the deep sedimentary subbasin Baiyun Sag bounded by low angle extensional faults soling out at midcrustal level.

LCHVA were detected around the Baiyun Sag with variable thicknesses of 5–8 km (Huang et al., 2005; Yan et al., 2001). Syn-rift

magmatism was also weak in the Baiyun Sag. Magmatic activities documented by BY7-1-1 well occurred in two episodes, 23.8 Ma and 17.6 Ma, mainly in volcanic mounds, sills and lava flows (Zhao et al., 2016). However, large-scale magmatic seamounts due to post-rift extrusion develop at the seaward side of the Baiyun Sag (Zhu et al., 2012).

3.3. The Xisha Trough

Commonly regarded as an abandoned rift, the W-E elongated Xisha Trough laterally extends over a distance of more than 400 km (Fig. 1b) (Lei and Ren, 2016; Qiu et al., 2001). The initial extension is proposed at three possible ages: 40.4 Ma (Hu et al., 2013), 44 Ma (Xie et al., 2006), or 54 Ma (Morley, 2016). Its rifting evolution is closely linked to the seafloor spreading of the Northwest Subbasin to the east (Qiu et al., 2001; Shi et al., 2002; Taylor and Hayes, 1980, Taylor and Hayesb, 1983).

In profile L3 (Fig. 4), the minimum time interval between the basement reflector Tg and the Moho reflection is 0.2 s TWTT. Assuming an average crustal velocity of 6.5 km/s, the extremely extended crust is only ~0.65 km in thickness. Most of the normal faults cut through the whole crust and sole into the mantle boundary. Mantle exhumation probably occurred in the Xisha Trough.

Different from the Baiyun Sag and Tainan Southern Depression where LCHVA are detected, no LCHVA was observed under the Xisha

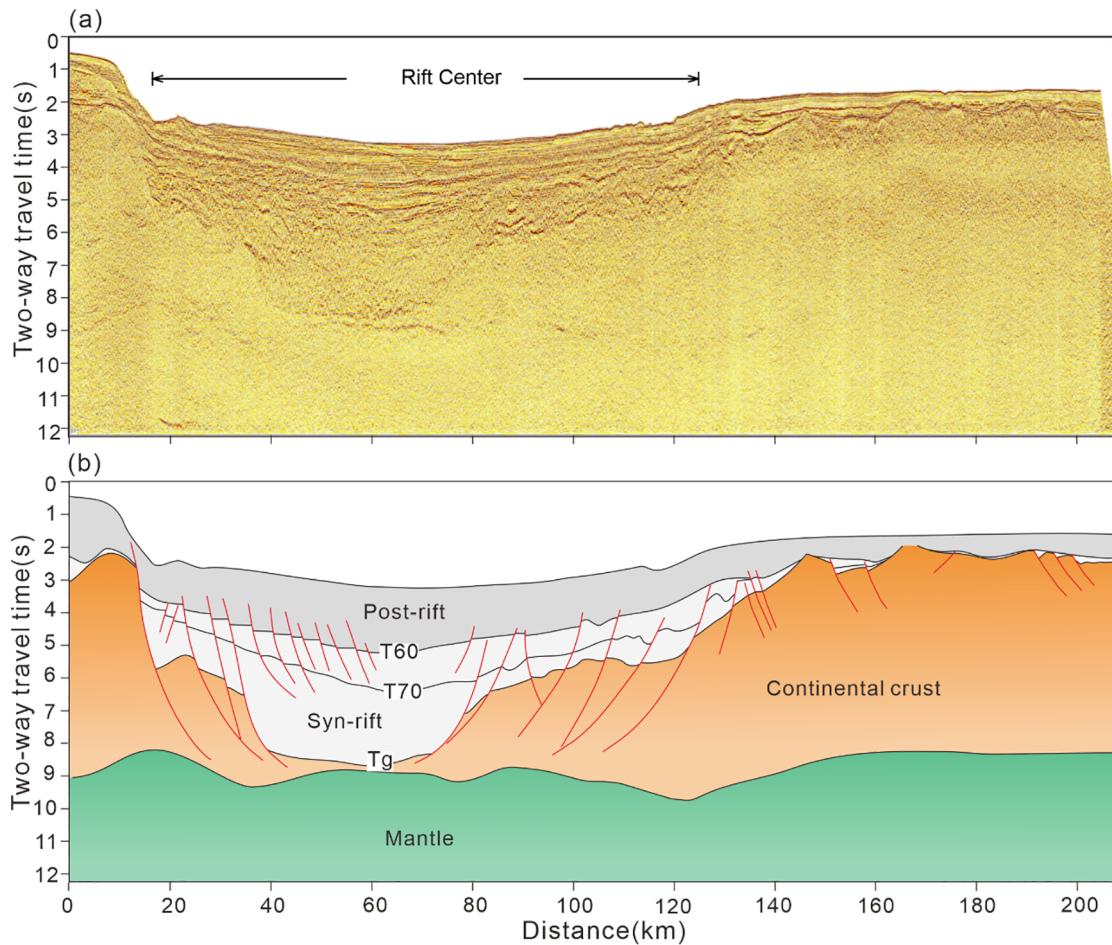


Fig. 4. (a) Seismic profile L3 across the Xisha Trough (modified from Gao et al., 2016). (b) Geological interpretation of the L3. T70: unconformity caused by seafloor spreading in ESB (~34 Ma); T60: breakup unconformity in SWSB (~23.6 Ma); Tg: top basement.

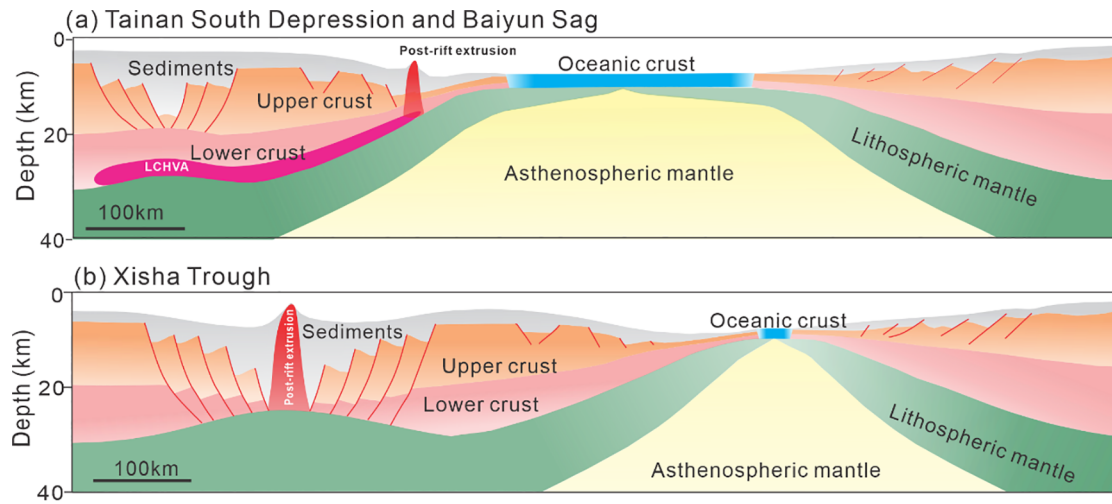


Fig. 5. The conceptual crustal structure diagrams showing the difference between (a) the Baiyun Sag and the Tainan Southern Depression and (b) the Xisha Trough. LCHVA: lower crust high velocity anomalies.

Trough (Qiu et al., 2001). Syn-rift magmatism was weak in the Xisha Trough. However, intensive post-rift magmatism penetrated through the Moho reflection and extruded/intruded overlaying sediment in the trough center (Fig. 1b) (Lei and Ren, 2016). Lei and Ren (2016) showed that the upper crust extension is substantially less than whole crust or whole lithosphere extension, and suggested the Cenozoic extension of the Xisha Trough is depth-dependent.

3.4. Comparison of failed rifts

Seismic profiles show that all three failed rifts along the northern SCS margin have hyper-thinned continental crust with weak syn-rift magmatic activity. However, their crust configurations and post-rift magmatic activities vary considerably.

In the Tainan Southern Depression and the Baiyun Sag, the upper

Table 1
Model material and thermal properties.

Property	Symbol	Value
Frictional-plastic parameters		
Cohesion (Pa)	C_{crust}	1×10^7
Cohesion after strain		0
Boundary cohesion		1000
Boundary friction cohesion		1000
Initial softening strain		0
Final softening strain		100
Crust wet quartz		
Power law exponent	n_{crust}	4.0
Activation energy(J/mol)	Q	223×10^3
Initial constant (Pa^{-n}/s)	A	8.574×10^{-28}
Activation volume(m^3/mol)	V	0
Density(kg/m^3)	ρ	2800
Low crust dry maryland diabase		
Power law exponent	n	4.7
Activation energy(J/mol)	Q	480×10^3
Initial constant (Pa^{-n}/s)	A	5.78×10^{-12}
Activation volume(m^3/mol)	V	0
Density (kg/m^3)	ρ	2800
Mantle wet olivine		
Power law exponent	n	3.0
Activation energy (J/mol)	Q	430×10^3
Activation volume (m^3/mol)	V	15×10^{-6}
Initial constant (Pa^{-n}/s)	A	1.7578×10^{-14}
Upper mantle density (kg/m^3)	ρ	3300
Lower mantle density (kg/m^3)	ρ	3300
Weak Zone		
Density (kg/m^3)	ρ	2800
Temperature and thermal parameters		
Moho temperature(°C)	T_m	550
Basic lithosphere temperature(°C)	T_l	1330
Diffusivity(m^2/s)	K	1×10^{-6}
Surface temperature(°C)	T_o	0
Geothermal gradient in sublithospheric mantle(°C/km)	dT	0.4
Coefficient of thermal expansion(°C)	α	2×10^{-5}
Radiogenic heating rates		0
Radiogenic timescales	λ	0
Universal gas constant (J/mol/°C)	R	8.314
Thickness conditions		
Base of crust(km)		35
Thickness of upper crust(km)		18
Thickness of lower crust (km)		17
Base mantle lithosphere(km)		100
Base upper mantle(km)		250
Numeric constants		
Nonlinear tolerance		1.0^{-5}
Linear tolerance		5.0^{-4}
Nonlinear minimum iteration		5
Nonlinear maximum iteration		200
Boundary conditions		
Half extension rate (cm/yr)	$V/2$	2
Top boundary condition		Stress free surface
Side boundary conditions		Free slip, normal velocity V
Basal boundary conditions		Free slip, zero normal velocity

crust is extremely thinned and/or removed in some places. Most detachment faults soled into the upper-lower crust boundary. There are weak syn-rift magmatic activities in the central rift valley but intensive post-rift magmatism has been documented at the seaward side of the rift center. LCHVA between 7.0 and 7.5 km/s are detected beneath the lower crust (Fig. 5a).

In contrast, the Xisha Trough has extremely thinned continental crust, close to 0 km in thickness in the central part. Normal faults cut

down into the crust-mantle boundary. Post-rift volcanism is intense in the rift valley (Fig. 5b) whereas LCHVA are absent.

Along-strike variations in the amount of stretched continental crust are large (by nearly a factor of two) along the northern SCS margin (Hayes and Nissen, 2005), indicating a rapid variation in extensional patterns. Extension rate, rheology and thermal structures are the main factors that affect the extension and breakup of continental lithosphere. In the following sections, we try to understand the effect of these different factors by numerical modeling.

4. Strategy of the numerical modeling

We use an Arbitrary-Lagrangian-Eulerian (ALE) finite element method that can solve two or three-dimensional problems related to orogeny, rifting and subduction (Fullsack, 1995).

4.1. Governing equations

The finite element model solves for 2D thermo-mechanically coupled, quasi-static force balanced, incompressible viscous-plastic creeping flows (Fullsack, 1995), as following:

$$\frac{\partial \sigma_{ij}}{\partial x_i} - \frac{\partial p}{\partial x_i} + \rho g = 0, \quad j = 1, 2 \quad (1)$$

where p is the pressure and x_i , ρ , g and σ_{ij} are the spatial coordinates, density, gravitational acceleration and associated stress tensor which is the sum of a deviatoric part τ , respectively. Stress tensor $\sigma_{ij} = -p\delta_{ij} + \sigma'_{ij} = -p\delta_{ij} + 2\eta_{eff}\dot{\epsilon}_{ij}$, in which the strain rate tensor is $\dot{\epsilon}_{ij} = \frac{1}{2}(\frac{\partial v_j}{\partial x_i} + \frac{\partial v_i}{\partial x_j})$.

For non-Newtonian, there is a strain rate dependent rheology. It assumes that the material obeys the relation:

$$\dot{\epsilon} = A\tau^n \exp\left(-\frac{Q + PV}{RT}\right) \quad (2)$$

where n is the power-law exponent, A the pre-exponential scaling factor, Q the activation energy, V the activation volume, p the pressure, T the absolute temperature and R the universal gas constant. A , n , Q and V are derived from laboratory experiments (Table 1).

The viscous constitutive laws in terms of the strain rate is:

$$\tau = 2\eta\dot{\epsilon} \quad (3)$$

where η is the viscosity.

We can write the viscosity based on equations and as:

$$\eta = \frac{1}{2}A^{-1/n}(\dot{\epsilon}')^{(1-n)/n} \exp\left[\frac{Q + VP}{nRT}\right] \quad (4)$$

We also consider the energy conservation. The two-dimensional thermal structure is governed by the energy balance equation:

$$\rho C_p \left(\frac{\partial T_k}{\partial t} + v_i \frac{\partial T_k}{\partial x_i} \right) = \kappa \frac{\partial}{\partial x_i} \frac{\partial T_k}{\partial x_i} + \rho H \quad (5)$$

where C_p is the heat capacity at constant pressure, T_k the absolute temperature, t the time, κ the thermal conductivity, H the radiogenic heat production per unit mass and α the thermal expansion coefficient. The mechanical and thermal systems are coupled with the temperature and are solved sequentially during each model time-step.

Frictional-plastic (Drucker-Prager) yielding occurs when:

$$\sigma_y = (J'_2)^{1/2} = C \cos \phi_{eff} + p \sin \phi_{eff} \quad (6)$$

where $J'_2 = \frac{1}{2}\dot{\sigma}'_{ij}\dot{\sigma}'_{ij}$ is the second invariant of the deviatoric stress, ϕ_{eff} is the effective internal angle of friction, and C is cohesion.

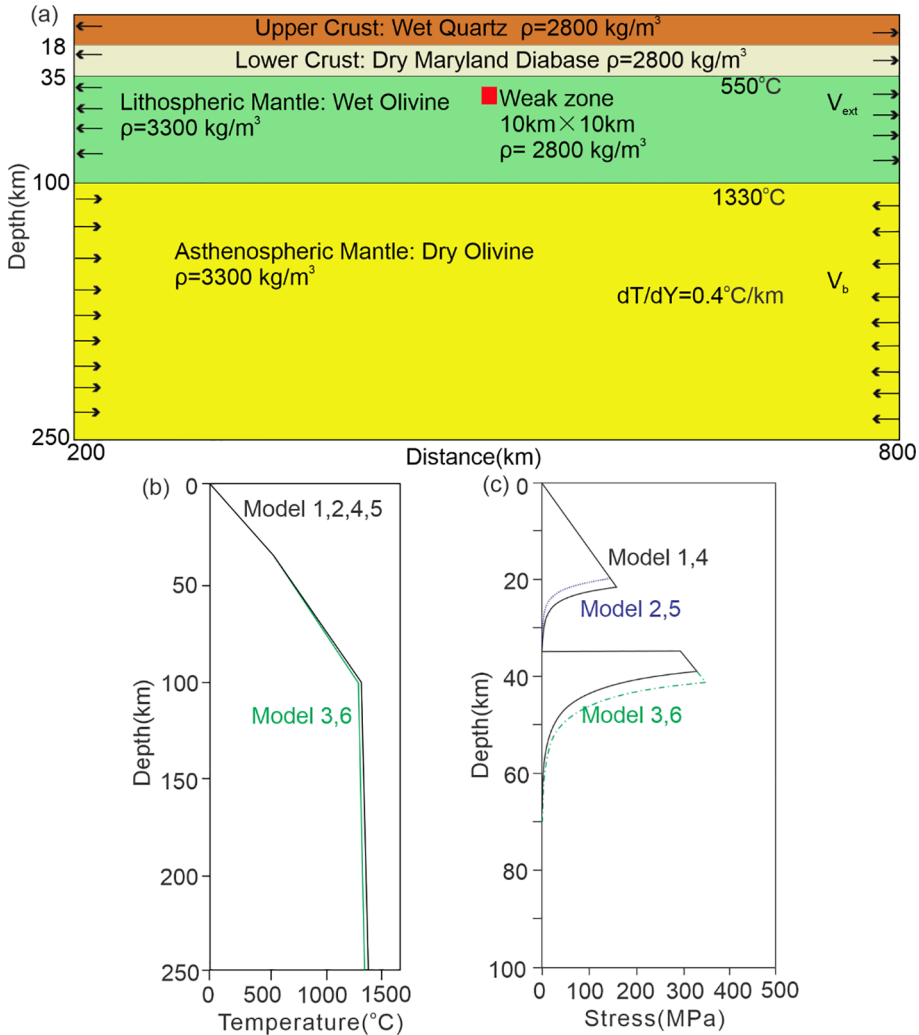


Fig. 6. (a) The initial numerical model setup showing the weak seed (red square) and the velocity boundary conditions, V_{ext} and V_b , which are chosen to achieve a mass balance in the system. The model has a free top surface. Other boundaries have zero tangential stress. Grid numbers in the horizontal and vertical dimension, n_x , n_y , are 101 and 49, respectively. The initial temperature field is laterally uniform and increases with depth from the surface, $T_0 = 0^\circ\text{C}$, to the base of crust, $T_m = 550^\circ\text{C}$. The temperature increases linearly with depth in the mantle lithosphere and the sublithospheric mantle is isothermal at $T_a = 1330^\circ\text{C}$. Thermal diffusivity is $1 \times 10^{-6} \text{ m}^2/\text{s}$. Crust and mantle densities are 2800 kg/m^3 and 3300 kg/m^3 , respectively. To avoid edge effects, the model is extended by more than 200 km each side (not shown here). (b) Thermal structure and (c) rheological stratification of models.

Table 2
Model testing parameters.

Model	Lower crust $A \text{ Pa}^{-n/s}$	Lithospheric base temperature $^\circ\text{C}$	Half extension rate cm/yr
1	5.78×10^{-12}	1330	2
2	5.78×10^{-10}	1330	2
3	5.78×10^{-12}	1300	2
4	5.78×10^{-12}	1330	1.5
5	5.78×10^{-10}	1330	1.5
6	5.78×10^{-12}	1300	1.5

4.2. Model setup

In setting up our initial model, we refer to the model parameters for the non-volcanic Iberia-Newfoundland continental margin (Huismans and Beaumont, 2014). The four-layer rheological model involves a granitic upper crust, a quartz diorite lower crust, an olivine upper mantle and sub-lithospheric mantle (Fig. 6). The thickness of the lithospheric mantle and crust is 65 km and 35 km, respectively. In the absence of well-constrained pre-rift lithosphere structure, we begin with the simple assumption that the pre-rift crust was uniform thickness over the entire South China. The lithosphere is laterally uniform except

for a small weak seed to localize deformation in the uppermost mantle.

Because the continental lithospheric extension and breakup is a complex process, the extension rate could vary with time and space. In this work, our numerical modeling mainly aimed at the formation of failed rifts. To roughly calculate the extensional rate, some assumptions are proposed. The extension rate was assumed essentially constant during rifting. It is not possible to directly measure the lithospheric thinning, and the crustal thinning will be assumed to reflect the whole lithospheric thinning. The amount of crustal thinning attributed to rifting can be estimated by comparing the present crustal thickness to the presumed thickness of pre-rift thickness. The extensional rate can be measured by dividing the width of stretched continental crust by the extensional duration time. Since the LCHVA were related to post-rifting underplating, we also consider that no new materials were added to the pre-rift continental crust during or after rifting.

The horizontal extension of continental crust is about 264–286 km wide in the eastern side of Zhongnan Fault (Bai et al., 2020). The rifting duration of Pearl River Mouth Basin is proposed from 15 to 20 Ma (Wang et al., 2018; Zhou et al., 1995), so the average half extensional velocity in the northern SCS is 1.32–1.91 cm/yr. In a previous study, the half extensional rate was given at about 0.4 cm/yr (Brune et al., 2017) but Bai et al. (2020) proposed that it was ~0.3 cm/yr when rifting initiated, and the maximum value reached as estimated 4.3 cm/

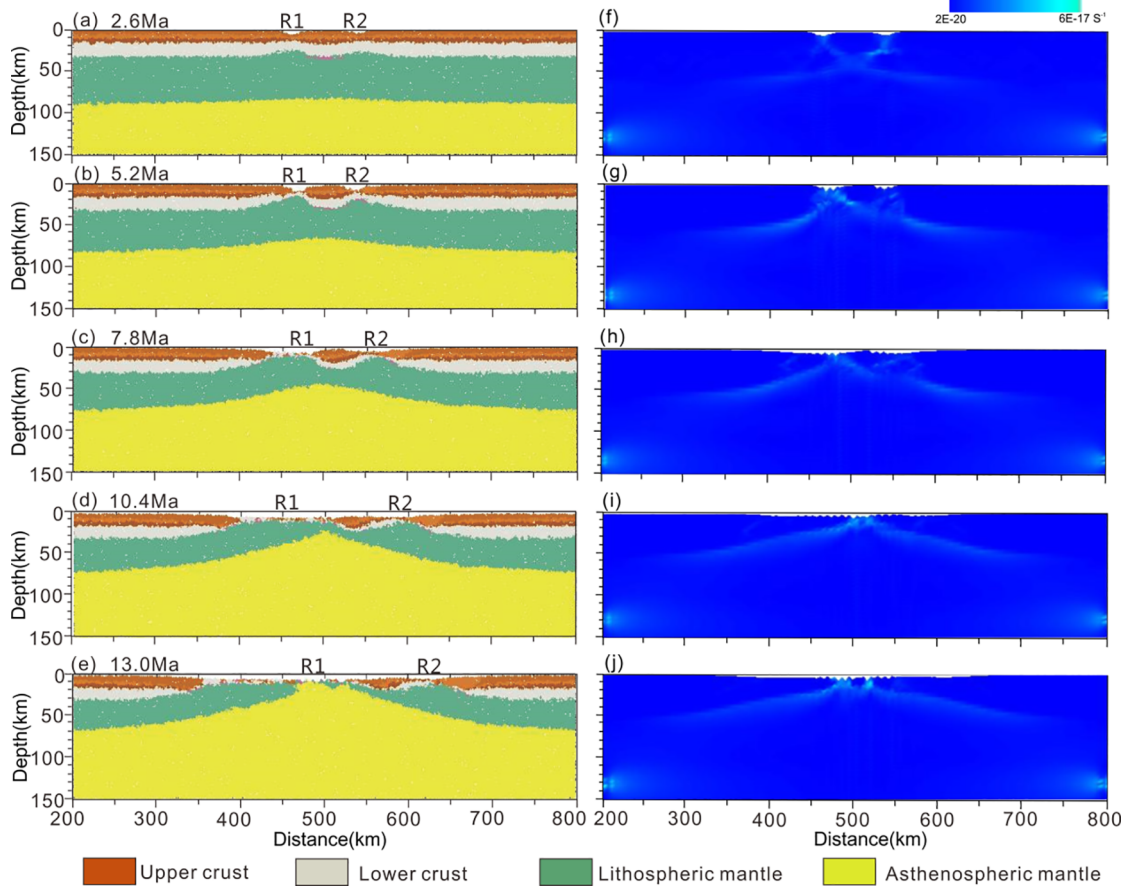


Fig. 7. Dynamic evolution of model 1. Panels on the left (a, b, c, d, e) are the structural evolution models and on the right (f, g, h, i, j) are corresponding strain rates, respectively. R1 and R2 are rift valleys.

yr before continental breakup based on plate restoration analysis.

Previous studies suggested that the SCS has a weak lower crust (Brune et al., 2017; Song, 2016; Song et al., 2019), which is adopted in our initial model. The thermal and mechanical characteristics of each material are summarized in Table 1.

To illustrate the primary control factors on the rifting style and the evolution of continental breakup process, we design a series of models with different lower crust rheologies which are obtained by modifying the parameter A in equation, lithosphere temperatures and extension rates (Table 2). Extension is achieved by applying velocity boundary conditions and seeded by the small plastic weak region (Fig. 6a).

5. Numerical modeling results

5.1. Model 1

The extensional evolution of model 1 can be partitioned into two phases. The first stage is dominated by localized symmetrical brittle extension of the continental crust in two symmetric frictional-plastic shear zones (R1 and R2) (0–5.2 Ma; Fig. 7a, b, f, and g). The second stage (7.8–13.0 Ma; Fig. 7c, d, and e) is characterized by asymmetrical ductile extension of the lithospheric mantle and asthenosphere. Starting from 5.2–7.8 Ma, rifting competition between R2 and R1 occurs and the strain preferentially focuses on R1 (Fig. 7g). Eventually, continental breakup and seafloor spreading occurs at R1 (Fig. 7d and i) and in

contrast, R2 is abandoned with a hyper-extended continental crust. Continental crustal blocks are attenuated between R1 and R2. The two conjugate continental margins of R1 have pronounced difference in width, geometry and structural style (Fig. 7e and g). The right margin is featured with a narrow transition zone, but the left margin shows a very wide and extremely thinned continental crust.

5.2. Model 2

Model 2 is the same as model 1 except that in the lower crust A is $5.78 \times 10^{-10} \text{ Pa}^{-n}/\text{s}$. The tectonic style of deformation again involves two different phases. Phase one (0–5.2 Ma; Fig. 8a and b) is similar to that of model 1, but unlike the strain localization in rift valley in model 1, as the extension proceeds, strain in model 2 is discrete and crustal deformation is more diffused between R1 and R2 (7.8–15.6 Ma; Fig. 8). Eventually the rift feature of R2 disappears and hyper-extended continental crust occurs in very wide zones (Fig. 8d and i). At 15.6 Ma, the lithosphere breaks up at R1 (Fig. 8e). In this model, the continental crust and mantle lithosphere breakup simultaneously and no failed rift is stabilized along the continental margin.

5.3. Model 3

Model 3 is the same as Model 1, except that the base temperature of the lithosphere is 30 °C lower. This model is similar in early evolution

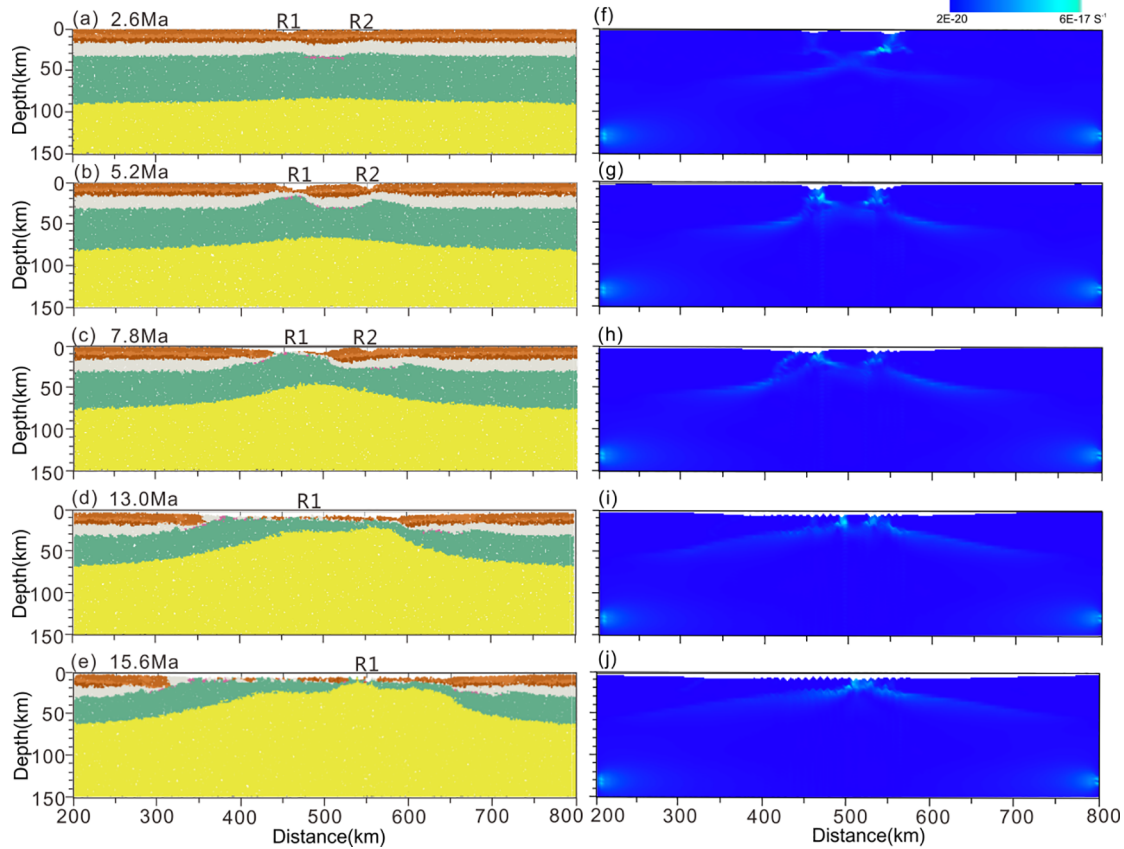


Fig. 8. Dynamic evolution of model 2. Panels on the left (a, b, c, d, e) are the structural evolution models and on the right (f, g, h, i, j) are their corresponding strain rates, respectively. R1 and R2 are rift valleys. See Fig. 7 for color legend.

process with models 1 and 2. Lithosphere thinning and asthenosphere upwelling are symmetric (Fig. 9b and c), but again no failed rift develops along the continental margin (Fig. 9e). Mantle lithosphere appears directly exposed in the ocean-continent transition zone. Models 2 and 3 are inconsistent with our observation of failed rifts along the northern SCS margin.

5.4. Model 4

Model 4 is the same with model 1 except that the half extensional rate is decreased to 1.5 cm/yr. The initial extension takes longer than model 1 due to the lower extension rate (Fig. 10a). Unlike previous models with two conjugate frictional-plastic shear zones developed on the shoulders of the weak zone (Fig. 7a), deformation concentrates on one primary rift R1 at the beginning (Fig. 10b and c). At 16.7 Ma, as extension continues, asymmetric asthenosphere upwelling occurs (Fig. 10d and e). Mantle thinning and final breakup start to concentrate in a new location different from the initial extensional center R2 (Fig. 10d), while the early rift valley R1 becomes abandoned. Rift migration is enabled by initial fault asymmetry as well as relatively weak crust, leading to a high degree of margin asymmetry. In this model, the width of abandoned rift R1 is about 50–60 km (Fig. 10e).

5.5. Model 5

Model 5 is the same as model 4 except that in lower crust A is $5.78 \times 10^{-10} \text{ Pa}^{-n}/\text{s}$, and this reduced rheology slows down the evolution pace. Phase one (0–13.4 Ma) is featured with symmetric deformation and asthenosphere uplifting (Fig. 11a, b and c). All the deformation is localized on one frictional-plastic rift center R1 (Fig. 11a), causing extreme crustal thinning (Fig. 11b) and mantle exhumation (Fig. 11c).

In phase two, mantle lithosphere extension is asymmetric (Fig. 11d), rift center migrates to R2 at 16.7 Ma (Fig. 11d), and the final breakup achieves at 23.1 Ma (Fig. 11e). Asymmetric rifting generates a hyper-extended continental crust of ~200 km wide to the right and ~80 km wide to the left of the final rifting center (Fig. 11e). The difference between model 5 and model 4 is in the location of the lithosphere rupture and the width of abandoned rift R1, which is about 100 km (Fig. 11d).

5.6. Model 6

The temperature at the lithospheric base of model 6 is reduced by 30 °C from model 4. Model 6 is much similar to model 4 in evolution, but the width of exhumed mantle in R1 is about 100 km (Fig. 12e).

Models 5 and 6 have wide exhumed mantle zones (about 100 km),

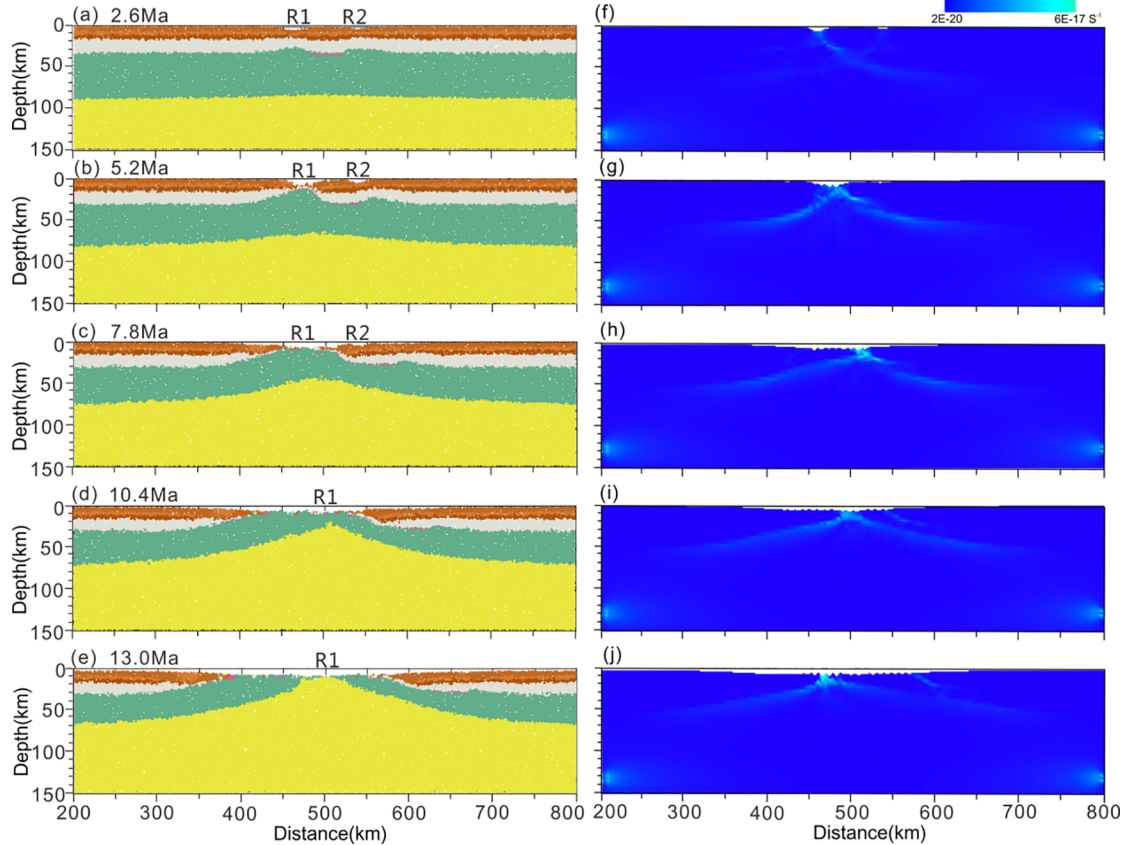


Fig. 9. Dynamic evolution of model 3. Panels on the left (a, b, c, d, e) are the structural evolution models and on the right (f, g, h, i, j) are corresponding strain rates, respectively. R1 and R2 are rift valleys. See Fig. 7 for color legend.

which are not conformable to seismic observations in the SCS (Fig. 4). We conclude that models 1 and 4 match well with our observations in the SCS.

6. The formation of failed rifts in the SCS

Our numerical modeling identifies two types of formation mechanism for failed rifts: syn-rift competitive type (Fig. 13a; model 1) and rift migration type (Fig. 13b; model 4). Rift migration is caused by cooling and strengthening of mantle material at the exhumed mantle and simultaneous weakening at the new rift valley due to conductive heat from the hot asthenospheric upwelling (Brune et al., 2017; Brune et al., 2014; Liao and Gerya, 2014). Both processes generate a lateral strength contrast that leads to migration of the rift centre, as observed in model 4 (Fig. 10e). In this type, the failed rift R1 is not competing with R2 forming the middle ocean ridge (Fig. 13b).

These hyper-extended failed rifts in the northern SCS margin did not breakup, due to differential extension of the crust and mantle lithosphere. Model 4 (Fig. 10e) shows that the continental crust is almost torn apart at R1, but the lithospheric mantle is not thinned enough. The final continental breakup occurs at R2. It implies that depth-dependent lithospheric extension caused failed rifts in the SCS.

The northern SCS margin shows dramatic along-strike heterogeneity, in heat flow (Nissen et al., 1995a; Nissen et al., 1995b), width of extended continental crust (Hayes and Nissen, 2005) and lower-crust high-velocity layer (Qiu et al., 2001; Yan et al., 2001). In this study, we

also demonstrate that the abandoned rifts in the eastern segment (the Baiyun Sag and the Tainan Southern Depression) are dissimilar to the Xisha Trough to the west.

Rift migration may have formed the Xisha Trough, the longest failed rift system in the northern SCS margin. Seafloor spreading propagated from the east to west during the early Oligocene, but failed in the Xisha Trough and spreading center subsequently jumped southwards. The final breakup and seafloor spreading occurred in a new rift center to the south of the Xisha Trough. In model 4, normal faults cut through the continental crust, which is torn apart and the rift center spans about 50–60 km (Fig. 10e). These similar features are present on the seismic profile in the Xisha Trough (Fig. 4).

Compared with the Xisha Trough, the Baiyun Sag and Tainan Southern Depression have smaller extension scale and different fault patterns. No rift migration has been detected in these areas. In the seismic profiles, the continental crusts are not full torn apart, and are formed more likely by rift competition.

Hayes and Nissen (2005) used different models with varying rift zone widths and initial crustal thicknesses to examine the rifting and seafloor spreading history of northern SCS margin. They excluded extension rate as a potential factor causing east-west rifting variations. However, they ignored failed rifts in their study and proposed that failed rifts have little impact on analysis of the integrated crustal extension across and along the rifted margin of South China.

Nirrengarten et al. (2020) proposed that the hyper-extended crust in northern SCS margin resulted from a heterogeneous and likely

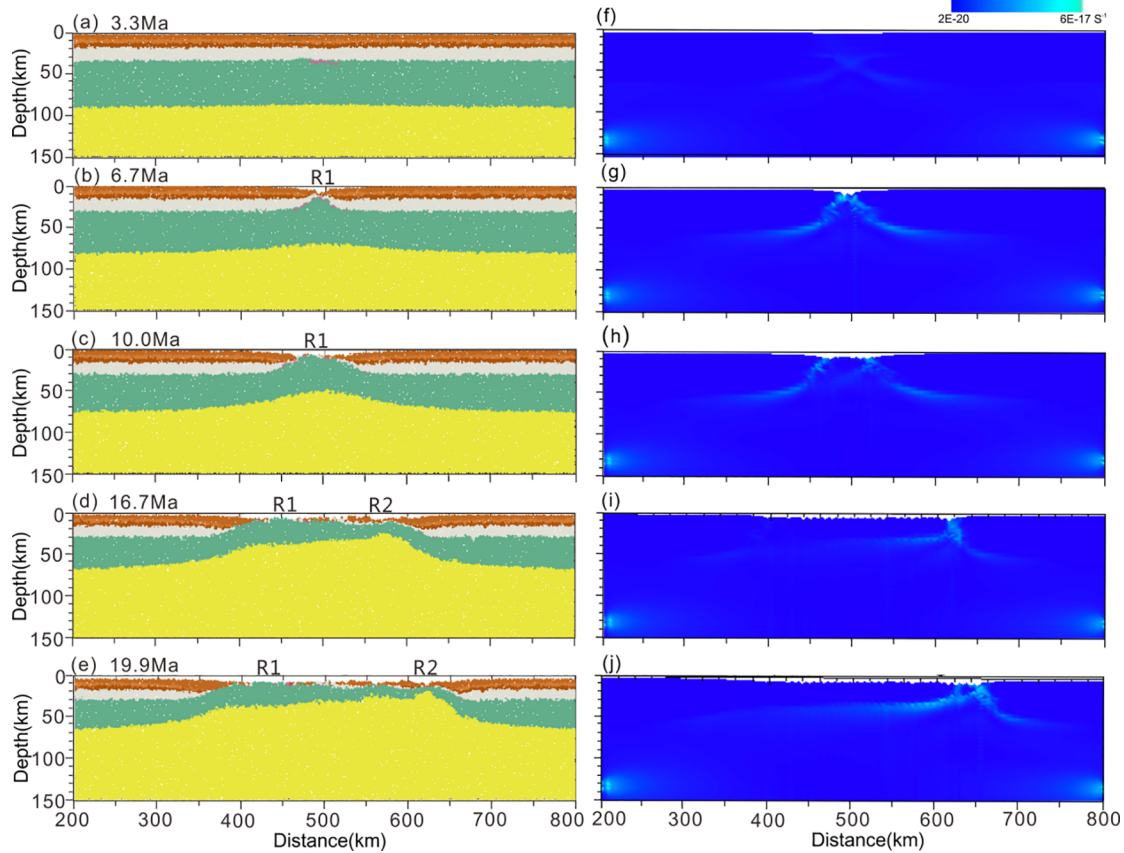


Fig. 10. Dynamic evolution of model 4. Panels on the left (a, b, c, d, e) are the structural evolution models and on the right (f, g, h, i, j) are corresponding strain rates, respectively. R1 and R2 are rift valleys. See Fig. 7 for color legend.

thermally un-equilibrated lithosphere formed by the Mesozoic Yen-shanian orogeny. Geologically more realistic numerical modeling with natural inheritance will be required to test this idea. Pre-rift inherited weak zones from the late Mesozoic subduction could form failed rifts. Chenin and Beaumont (2013) investigated the reactivation of inherited offset weak zones during continental rifting and breakup based on numerical modeling. They proposed that the formation of offset rift basins depends on the competition between necking instabilities at the weak zones in the stiff layers, and the coupling between the stiff and pliable layers. Not all pre-existing weak zones will be reactive during extension.

Our numerical modeling shows that the extension rate is a significant parameter to affect the geometrical evolution of continental margin, especially in the formation of failed rift. The syn-rift competitive type (the Baiyun Sag and Tainan Southern Depression) requires a higher extension rate than the rift migration type (the Xisha Trough). These required extensional rates are consistent with calculations from the thinned continental crust and the rifting duration. The eastern segment appears to have a faster extension rate than the western segment of the northern SCS margin.

The difference of extension rates between the eastern and western SCS is further supported by the Zhongnan Fault Zone (Fig. 1). This zone

is oriented N-S, parallel to the extension and seafloor spreading direction, and acted as a major transform boundary between the East and Southwest Subbasins (Yao, 1995).

It is worth noting that our initial model (Fig. 6) assumes a low rheology of the lower crust in the SCS. On this rheology, the extension rate plays a large role in causing the difference between the eastern and western segments of the continental margin.

7. Conclusion

Our study draws the following conclusions:

- (1) All the studied failed rifts show hyper-extended continental crust, but are diverse in crustal configurations, developments of LCHVA and tectonic styles of detachment faults. The Baiyun Sag and the Tainan Southern Depression have LCHVA and intracrust low-angle detachment faults. In contrast, the Xisha Trough, as the longest and largest failed rift system in the northern SCS margin, shows extremely thinned continental crust (close to 0 km in the central trough), absence of LCHVA, and normal faults mostly cut through the crust-mantle boundary.
- (2) Through numerical simulation, we revealed two possible formation

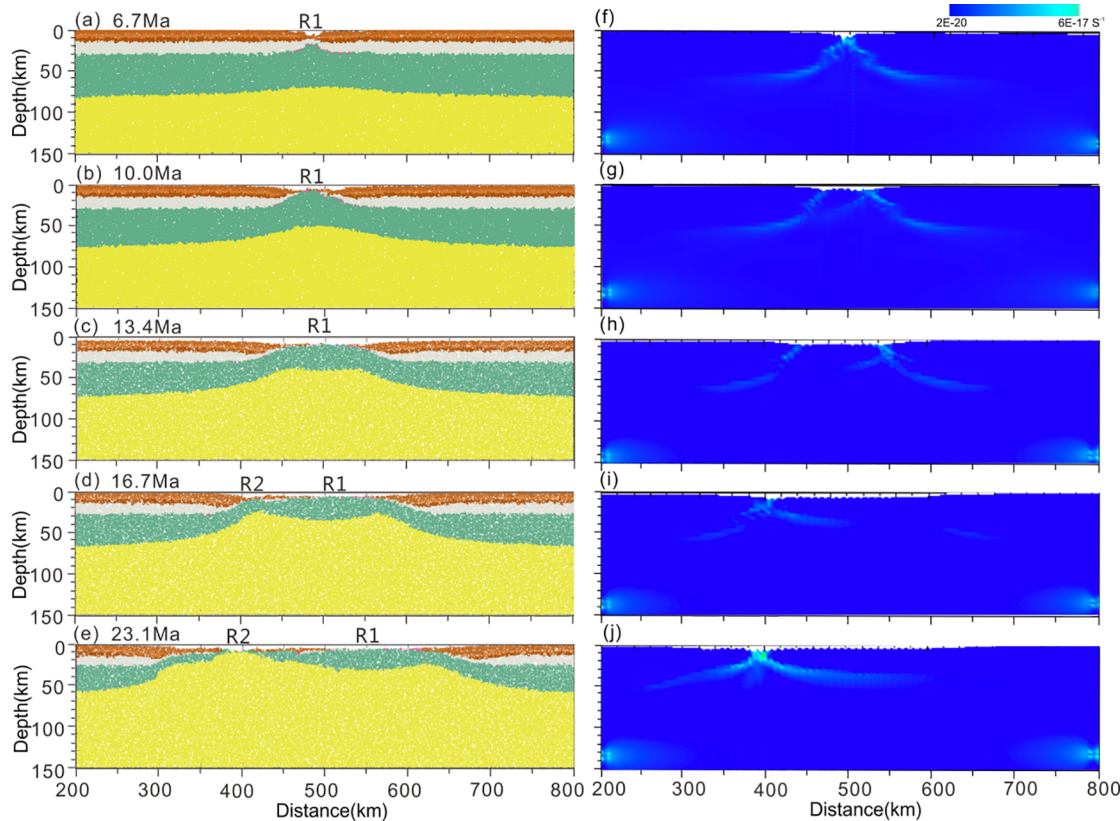


Fig. 11. Dynamic evolution of model 5. Panels on the left (a, b, c, d, e) are the structural evolution models and on the right (f, g, h, i, j) are corresponding strain rates, respectively. R1 and R2 are rift valleys. See Fig. 7 for color legend.

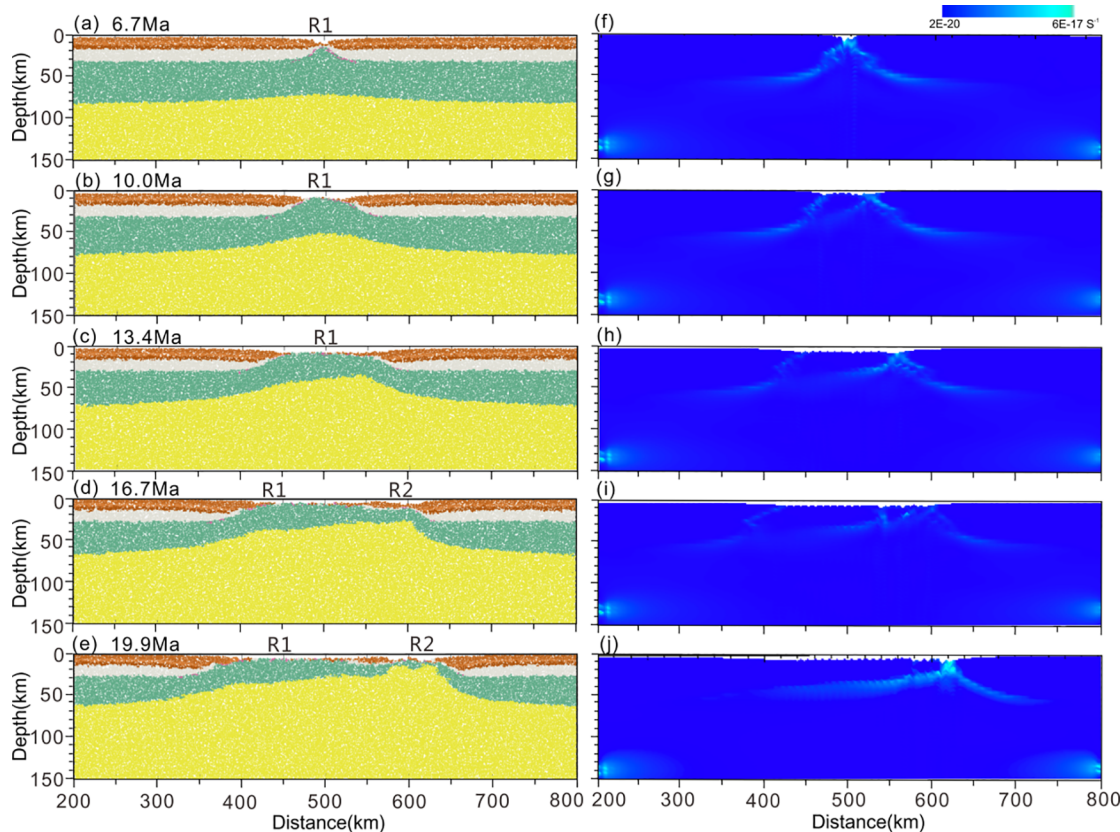


Fig. 12. Dynamic evolution of model 6. Panels on the left (a, b, c, d, e) are the structural evolution models and on the right (f, g, h, i, j) are corresponding strain rates, respectively. R1 and R2 are rift valleys. See Fig. 7 for color legend.

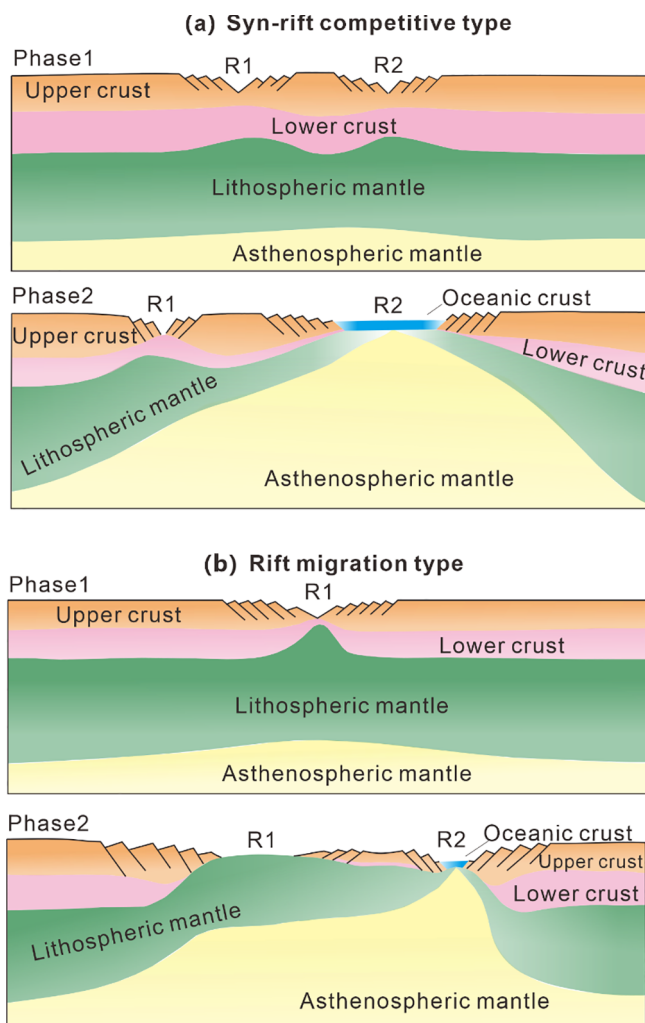


Fig. 13. Conceptual diagrams illustrating the proposed formation mechanisms of failed rifts based on the numerical modeling results. (a) syn-rift competitive type; (b) rift migration type. R1: Rift 1; R2: Rift 2.

mechanisms of the abandoned rifts with different extension rates: the rift competitive type and the rift migration type. The Baiyun Sag and Tainan Southern Depression likely belong to the syn-rift competitive type whereas the Xisha Trough probably belongs to the rift migration type.

(3) The continental rifting and breakup of the SCS is a depth-dependent process. The tectonic difference between the eastern and western margins may be primarily due to different extension rates, in addition to the lithosphere thermal state and the rheology of the lower crust.

CRediT authorship contribution statement

Yaqing Li: Conceptualization, Writing - original draft. **Aqeel Abbas:** . Chun-Feng Li: Conceptualization, Supervision. **Tienan Sun:** Software. **Sergio Zlotnik:** Software. **Taoran Song:** . Lulu Zhang: . Zewei Yao: . Yongjian Yao: .

Declaration of Competing Interest

The authors declare that they have no known competing financial interests or personal relationships that could have appeared to influence the work reported in this paper.

Acknowledgments

This work was funded by National Natural Science Foundation of China, China (grant number: 41761134051 and 41706046). We would like to thank Jinwei Gao from the Institute of Deep-sea Science and Engineering, Chinese Academy of Sciences and Yanghui Zhao from the Second Institute of Oceanography, State Oceanic Administration, Ministry of Natural Resources, China for sharing the high resolution seismic sections. We are grateful to Pin Yan from the South China Sea Institute of Oceanology, Chinese Academy of Sciences, for his helpful suggestions. We are also grateful for the critical but constructive comments by Andrew Cullen and two anonymous reviewers.

Appendix A. Supplementary material

Supplementary data to this article can be found online at <https://doi.org/10.1016/j.jseas.2020.104402>.

References

- Allken, V., Huismans, R.S., Thieulot, C., 2011. Three-dimensional numerical modeling of upper crustal extensional systems. *J. Geophys. Res.* 116, B10409.
- Bai, Y., Wang, X., Dong, D., Brune, S., Wu, S., Wang, Z., 2020. Symmetry of the South China Sea conjugate margins in a rifting, drifting and collision context. *Mar. Pet. Geol.* 117, 104397.
- Barckhausen, U., Engels, M., Franke, D., Ladage, S., Pubellier, M., 2014. Evolution of the South China Sea: Revised ages for breakup and seafloor spreading. *Mar. Pet. Geol.* 58, 599–611.
- Barckhausen, U., Roeser, H.A., 2004. Seafloor spreading anomalies in the South China Sea revisited. In: Clift, P., Wang, P., Kuhnt, W., Hayes, D. (Eds.), *Continent–Ocean Interactions with East Asian Marginal Seas*. American Geophysical Union, vol. 140, pp. 121–125.
- Boillot, G., Grimaud, S., Mauffret, A., Mougenot, D., Kornprobst, J., Mergoil-Daniel, J., Torrent, G., 1980. Ocean-continent boundary off the Iberian margin: a serpentinite diapir west of the Galicia Bank. *Earth Planet. Sci. Lett.* 48, 23–34.
- Braigis, A., Patriat, P., Tapponnier, P., 1993. Updated interpretation of magnetic anomalies and seafloor spreading stages in the south China Sea: implications for the Tertiary tectonics of Southeast Asia. *J. Geophys. Res. Solid Earth* 98, 6299–6328.
- Brune, S., Heine, C., Clift, P.D., Pérez-Gussinyé, M., 2017. Rifting margin architecture and crustal rheology: reviewing Iberia-Newfoundland, Central South Atlantic, and South China Sea. *Mar. Pet. Geol.* 79, 257–281.
- Brune, S., Heine, C., Pérez-Gussinyé, M., Sobolev, S.V., 2014. Rift migration explains continental margin asymmetry and crustal hyper-extension. *Nat. Commun.* 5, 4014.
- Chenin, P., Beaumont, C., 2013. Influence of offset weak zones on the development of rift basins: activation and abandonment during continental extension and breakup. *J. Geophys. Res. Solid Earth* 118, 1698–1720.
- Chian, D., Loudon, K.E., 1994. The continent-ocean crustal transition across the southwest Greenland margin. *J. Geophys. Res.* 99, 9117–9135.
- Clift, P., Lee, G.H., Nguyen, A.D., Barckhausen, U., Long, H., Zhen, S., 2008. Seismic reflection evidence for a Dangerous Grounds miniplate: no extrusion origin for the South China Sea. *Tectonics* 27, 1–16.
- Clift, P., Lin, J., Barckhausen, U., 2002. Evidence of low flexural rigidity and low viscosity lower continental crust during continental break-up in the South China Sea. *Mar. Pet. Geol.* 19, 951–970.
- Cullen, A., 2014. Reprint: nature and significance of the west baram and tinjar lines, NW Borneo. *Mar. Pet. Geol.* 58, 674–686.
- Cullen, A., Reemst, P., Henstra, G., Gozzard, S., Ray, A., 2010. Rifting of the South China Sea: new perspectives. *Pet. Geosci.* 16, 273–282.
- Ding, W.-W., Li, J.-B., Li, M.-B., Qiu, X.-L., Fang, Y.-X., Tang, Y., 2008. A Cenozoic tectono-sedimentary model of the Tainan Basin, the South China Sea: evidence from a multi-channel seismic profile. *J. Zhejiang Univ.-Sci. A* 9, 702–713.
- Franke, D., Barckhausen, U., Heyde, I., Tingay, M., Ramli, N., 2008. Seismic images of a collision zone offshore NW Sabah/Borneo. *Mar. Pet. Geol.* 25, 606–624.
- Fulsack, P., 1995. An arbitrary lagrangian-eulerian formulation for creeping flows and its application in tectonic models. *Geophys. J. Int.* 120, 1–23.
- Gao, J., Wu, S., McIntosh, K., Mi, L., Yao, B., Chen, Z., Jia, L., 2015. The continent–ocean transition at the mid-northern margin of the South China Sea. *Tectonophysics* 654, 1–19.
- Gao, J.W., Wu, S.G., McIntosh, K., Mi, L.J., Liu, Z., Spence, G., 2016. Crustal structure and extension mode in the northwestern margin of the South China Sea. *Geochem. Geophys. Geosyst.* 17, 2143–2167.
- Hall, R., 2002. Cenozoic geological and plate tectonic evolution of SE Asia and the SW Pacific: computer-based reconstructions, model and animations. *J. Asian Earth Sci.* 20, 353–431.
- Hall, R., 2012. Late JurassiceCenozoic reconstructions of the Indonesian region and the Indian Ocean. *Tectonophysics* 570, 1–43.
- Hauser, F., O'Reilly, B.M., Jacob, A.W.B., Shannon, P.M., Makris, J., Vogt, U., 1995. The crustal structure of the Rockall Trough: Differential stretching without underplating. *J. Geophys. Res. Solid Earth* 100, 4097–4116.
- Hayes, D.E., Nissen, S.S., 2005. The South China sea margins: implications for rifting

- contrasts. *Earth Planet. Sci. Lett.* 237, 601–616.
- Hinz, K., Fritsch, J., Kempfer, E.H.K., Manaf Mohammad, A., Meyer, J., Vosberg, D.M.H., Benavidez, J.W.J., 1989. Thrust tectonics along the north-western continental margin of Sabah/Borneo. *Geologische Rundschau* 78, 705–730.
- Holloway, N.H., 1982. north palawan block, philippines-its relation to asian mainland and role in evolution of south China sea. *AAPG Bull.* 66, 1355–1383.
- Hou, W., Li, C.F., Wan, X., Zhao, M.H., Qiu, X., 2019. Crustal S-wave velocity structure across the northeastern South China Sea continental margin: implications for lithology and mantle exhumation. *Earth Planetary Phys.* 3, 314–329.
- Hu, B., Wang, L., Yan, W., Liu, S., Cai, D., Zhang, G., Zhong, K., Pei, J., Sun, B., 2013. The tectonic evolution of the Qiongdongnan Basin in the northern margin of the South China Sea. *J. Asian Earth Sci.* 77, 163–182.
- Hu, D., Zhou, D., Wu, X., He, M., Pang, X., Wang, Y., 2009. Crustal structure and extension from slope to deepsea basin in the northern South China Sea. *J. Earth Sci.* 20, 27–37.
- Huang, C., Zhou, D., Sun, Z., Chen, C., Hao, H., 2005. Deep crustal structure of the Baiyun Rift, northern South China Sea revesled from deep seismic reflection profile. *Chin. Sci. Bull.* 50, 1131–1138.
- Huang, H., Qiu, X., Pichot, T., Klingelhoefer, F., Zhao, M., Wang, P., Hao, T., 2019a. Seismic structure of the northwestern margin of the South China Sea: implication for asymmetric continental extension. *Geophys. J. Int.* 218, 1246–1261.
- Huang, H., Qiu, X., Zhang, J., Hao, T., 2019b. Low-velocity layers in the northwestern margin of the South China Sea: Evidence from receiver functions of ocean-bottom seismometer data. *J. Asian Earth Sci.* 186, 104090.
- Huismans, R.S., Beaumont, C., 2003. Symmetric and asymmetric lithospheric extension: relative effects of frictional-plastic and viscous strain softening. *J. Geophys. Res. Solid Earth* 108, 2496.
- Huismans, R.S., Beaumont, C., 2011. Depth-dependent extension, two-stage breakup and cratonic underplating at rifted margins. *Nature* 473, 74–78.
- Huismans, R.S., Beaumont, C., 2014. Rifted continental margins: the case for depth-dependent extension. *Earth Planet. Sci. Lett.* 407, 148–162.
- Jahn, B.M., Chen, P.Y., Yen, T.P., 1976. Rb-Sr ages of granitic rocks in Southeastern China and their tectonic significance. *Geol. Soc. Am. Bull.* 87, 763–776.
- Lei, C., Ren, J., 2016. Hyper-extended rift systems in the Xisha Trough, northwestern South China Sea: implications for extreme crustal thinning ahead of a propagating ocean. *Mar. Pet. Geol.* 77, 846–864.
- Lester, R., Lavier, L.L., McIntosh, K., Van Avendonk, H.J.A., Wu, F., 2012. Active extension in Taiwan's precollision zone: a new model of plate bending in continental crust. *Geology* 40, 831–834.
- Lester, R., Van Avendonk, H.J.A., McIntosh, K., Lavier, L., Liu, C.S., Wang, T.K., Wu, F., 2014. Rifting and magmatism in the northeastern South China Sea from wide-angle tomography and seismic reflection imaging. *J. Geophys. Res. Solid Earth* 119, 2305–2323.
- Li, C.-F., Xu, X., Lin, J., Sun, Z., Zhu, J., Yao, Y.L., Zhao, X., Liu, Q., Kulhanek, D.K.e.a., 2014. Ages and magnetic structures of the South China Sea constrained by deep tow magnetic surveys and IODP Expedition 349. *Geochem. Geophys. Geosyst.* 15, 4958–4983.
- Li, C.-F., Zhou, Z., Li, J., Hao, H., Geng, J., 2007. Structures of the northeasternmost South China Sea continental margin and ocean basin: geophysical constraints and tectonic implications. *Mar. Geophys. Res.* 28, 59–79.
- Li, Z.-X., Li, X.-H., 2007. Formation of the 1300-km-wide intracontinental orogen and postorogenic magmatic province in Mesozoic South China: a flat-slab subduction model. *Geology* 35, 179.
- Liao, J., Gerya, T., 2014. Influence of lithospheric mantle stratification on craton extension: insight from two-dimensional thermo-mechanical modeling. *Tectonophysics* 631, 50–64.
- McIntosh, K., Lavier, L., van Avendonk, H., Lester, R., Eakin, D., Liu, C.-S., 2014. Crustal structure and inferred rifting processes in the northeast South China Sea. *Mar. Pet. Geol.* 58, 612–626.
- Mjelde, R., Raum, T., Myhren, B., Shimamura, H., Murai, Y., Takanami, T., Karpuz, R., Nass, U., 2005. Continent-ocean transition on the Voring Plateau, NE Atlantic, derived from densely sampled ocean bottom seismometer data. *J. Geophys. Res. Solid Earth* 110, B05101.
- Moresi, L., Dufour, F., Muhlhaus, H.B., 2003. A Lagrangian integration point finite element method for large deformation modeling of viscoelastic geomaterials. *J. Comput. Phys.* 184, 476–497.
- Morley, C.K., 2016. Major unconformities/termination of extension events and associated surfaces in the South China Seas: review and implications for tectonic development. *J. Asian Earth Sci.* 120, 62–86.
- Mutter, J.C., Talwani, M., Stoffa, P.L., 1984. Evidence for a thick oceanic crust adjacent to the Norwegian Margin. *J. Geophys. Res. Solid Earth* 89, 483–502.
- Nirrengarten, M., Mohn, G., Kusznir, N.J., Sapin, F., Despinois, F., Pubellier, M., Chang, S.P., Larsen, H.C., Ringenbach, J.C., 2020. Extension modes and breakup processes of the southeast China-Northwest Palawan conjugate rifted margins. *Mar. Pet. Geol.* 113, 104123.
- Nissen, S.S., Hayes, D.E., Bochu, Y., Zeng, W., Chen, Y., Nu, X., 1995a. Gravity, heat flow, and seismic constraints on the processes of crustal extension: Northern margin of the South China Sea. *J. Geophys. Res. Solid Earth* 100, 22447–22483.
- Nissen, S.S., Hayes, D.E., Buhl, P., Diebold, J., Bochu, Y., Zeng, W., Chen, Y., 1995b. Deep penetration seismic soundings across the northern margin of the South China Sea. *J. Geophys. Res. Solid Earth* 100, 22407–22433.
- O'Reilly, B.M., Hauser, F., Ravaut, C., Sgannon, P.M., Readman, P.W., 2006. Crustal thinning, mantle exhumation and serpentization in the Porcupine Basin, offshore Ireland: evidence from wide-angle seismic data. *J. Geol. Soc.* 163, 775–787.
- O'Reilly, B.M., Hauser, F., Jacob, A.W.B., Shannon, P.M., 1996. The lithosphere below the Rockall Trough: wide-angle seismic evidence for extensive serpentisation. *Tectonophysics* 255, 1–23.
- Pérez-Gussinyé, M., Morgan, J., Reston, T., Ranero, C., 2006. The rift to drift transition at non-volcanic margins: Insights from numerical modelling. *Earth Planet. Sci. Lett.* 244, 458–473.
- Qiu, X., Ye, S., Wu, S., Shi, X., Zhou, D., Xia, K., Flueh, E.R., 2001. Crustal structure across the Xisha Trough, northwestern South China Sea. *Tectonophysics* 341, 179–193.
- Reston, T.J., Gaw, V., Pennell, J., Klaeschen, D., Stubenrauch, A., Walker, I., 2004. Extreme crustal thinning in the south Porcupine Basin and the nature of the Porcupine Median High: implications for the formation of non-volcanic rifted margins. *J. Geol. Soc. Lond.* 161, 783–798.
- Savva, D., Meresse, F., Pubellier, M., Chamot-Rooke, N., Lavier, L., Po, K.W., Franke, D., Steuer, S., Sapin, F., Auxietre, J.L., Lamy, G., 2013. Seismic evidence of hyper-stretched crust and mantle exhumation offshore Vietnam. *Tectonophysics* 608, 72–83.
- Savva, D., Pubellier, M., Franke, D., Chamot-Rooke, N., Meresse, F., Steuer, S., Auxietre, J.L., 2014. Different expressions of rifting on the South China Sea margins. *Mar. Pet. Geol.* 58, 579–598.
- Shi, X., Kohn, B., Spencer, S., Guo, X., Li, Y., Yang, X., Shi, H., Gleadow, A., 2011. Cenozoic denudation history of southern Hainan Island, South China Sea: constraints from low temperature thermochronology. *Tectonophysics* 504, 100–115.
- Shi, X.B., Zhou, D., Qiu, X.L., Zhang, Y.X., 2002. Thermal and rheological structures of the Xisha Trough, South China Sea. *Tectonophysics* 351, 285–300.
- Song, T., 2016. The Crustal Structure and Lithosphere Rupture Mechanism of the Continental-ocean Transition Zone of the South China Sea. PhD thesis. Tongji University, Shanghai, China.
- Song, T., Li, C.-F., Wu, S., Yao, Y., Gao, J., 2019. Extensional styles of the conjugate rifted margins of the South China Sea. *J. Asian Earth Sci.* 177, 117–128.
- Tapponnier, P., Peltzer, G., Armijo, R., 1986. On the mechanisms of the collision between India and Asia. *Geol. Soc. Lond. Spec. Publ.* 19, 115–157.
- Tapponnier, P., Peltzer, G., Le Dain, A., Armijo, R., Cobbold, P., 1982. Propagating extrusion tectonics in Asia: new insights from simple experiments with plasticine. *Geology* 10, 611–616.
- Taylor, B., Hayes, D.E., 1980. The tectonic evolution of the South China Basin. In: Hayes, D.E. (Ed.), *The Tectonic and Geologic Evolution of Southeast Asian Seas and Islands: Part 1. Geophysical Monograph Series*, vol. 23, pp. 89–104.
- Taylor, B., Hayes, D.E., 1983. Origin and history of the South China Sea Basin. In: Hayes, D.E. (Ed.), *The Tectonic and Geologic Evolution of Southeast Asian Seas and Islands: Part 2. Geophysical Monograph Series*, vol. 27, pp. 23–56.
- Van Avendonk, H.J., Holbrook, W.S., Nunes, G.T., Shillington, D.J., Tucholke, B.E., Loudon, K.E., Larsen, H.C., Hopper, J.R., 2006. Seismic velocity structure of the rifted margin of the eastern Grand Banks of Newfoundland, Canada. *J. Geophys. Res. Atmos.* 111, B11404.
- van Wijk, J.W., Huismans, R.S., ter Voorde, M., Cloetingh, S.A.P.L., 2001. Melt generation at volcanic continental margins: No need for a mantle plume? *Geophys. Res. Lett.* 28, 3995–3998.
- Voss, M., Jokat, W., 2007. Continent-ocean transition and voluminous magmatic underplating derived from P-wave velocity modelling of the East Greenland continental margin. *Geophys. J. Int.* 170, 580–604.
- Wan, K., Xia, S., Cao, J., Sun, J., Xu, H., 2017. Deep seismic structure of the northeastern South China Sea: origin of a high-velocity layer in the lower crust. *J. Geophys. Res.: Solid Earth* 122.
- Wan, X., Li, C.F., Zhao, M., He, E., Liu, S., Qiu, X., Lu, Y., Chen, N., 2019. Seismic velocity structure of the magnetic quiet zone and continent-ocean boundary in the Northeastern South China Sea. *J. Geophys. Res. Solid Earth* 124, 11866–11899.
- Wang, J., Pang, X., Liu, B., Zheng, J., Wang, H., 2018. The Baiyun and Liwan Sags: two supradetachment basins on the passive continental margin of the northern South China Sea. *Mar. Pet. Geol.* 95, 206–218.
- Wang, T.K., Chen, M.-K., Lee, C.-S., Xia, K., 2006. Seismic imaging of the transitional crust across the northeastern margin of the South China Sea. *Tectonophysics* 412, 237–254.
- Wei, X.D., Zhao, M.H., Ruan, A.G., Qiu, X., Hao, T.Y., Wu, Z., Ao, W., Xiong, H., 2011. Crustal structure of shear waves and its tectonic significance in the mid-northern continental margin of the South China Sea. *Chin. J. Geophys.* 54, 3150–3160.
- Xie, X., Müller, R.D., Li, S., Gong, Z., Steinberger, B., 2006. Origin of anomalous subsidence along the Northern South China Sea margin and its relationship to dynamic topography. *Mar. Pet. Geol.* 23, 745–765.
- Yan, P., Deng, H., Liu, H., Zhang, Z., Jiang, Y., 2006. The temporal and spatial distribution of volcanism in the South China Sea region. *J. Asian Earth Sci.* 27, 647–659.
- Yan, P., Zhou, D., Liu, Z., 2001. A crustal structure profile across the northern continental margin of the South China Sea. *Tectonophysics* 338, 1–21.
- Yao, B., 1995. Characteristics and tectonic significance of the Zhongnan-Liyue fault. *Geological research of the South China Sea* (in Chinese). Memoir 7, 1–14.
- Yeh, Y.-C., Hsu, S.-K., Doo, W.-B., Sibuet, J.-C., Liu, C.-S., Lee, C.-S., 2012. Crustal features of the northeastern South China Sea: insights from seismic and magnetic interpretations. *Mar. Geophys. Res.* 33, 307–326.
- Zhao, F., Alves, T.M., Wu, S., Li, W., Huuse, M., Mi, L., Sun, Q., Ma, B., 2016. Prolonged

- post-rift magmatism on highly extended crust of divergent continental margins (Baiyun Sag, South China Sea). *Earth Planet. Sci. Lett.* 445, 79–91.
- Zhao, M., Qiu, X., Xia, S., Xu, H., Ping, W., Wang, T.K., Lee, C.S., Xia, K., 2010. Seismic structure in the northeastern South China Sea: S-wave velocity and Vp/Vs ratios derived from three-component OBS data. *Tectonophysics* 480.
- Zhao, Y., Ren, J., Pang, X., Yang, L., Zheng, J., 2018. Structural style, formation of low angle normal fault and its controls on the evolution of Baiyun Rift, northern margin of the South China Sea. *Mar. Pet. Geol.* 89, 687–700.
- Zhou, D., Ru, K., Chen, H.Z., 1995. Kinematics of cenozoic extension on the South China sea continental margin and its implications for the tectonic evolution of the region. *Tectonophysics* 251, 161–177.
- Zhu, J., Qiu, X., Kopp, H., Xu, H., Sun, Z., Ruan, A., Sun, J., Wei, X., 2012. Shallow anatomy of a continent-ocean transition zone in the northern South China Sea from multichannel seismic data. *Tectonophysics* 554–557, 18–29.